Mater. Res. Soc. Symp. Proc. Vol. 1297 © 2011 Materials Research Society
DOI: 10.1557/opl.2011.678

Nanometer Scale Mechanical Behavior of Grain Boundaries

Chien-Kai Wang, Huck Beng Chew, and Kyung-Suk Kim

School of Engineering, Brown University, Providence, RI 02912, U.S.A.

ABSTRACT

A nonlinear field projection method has been developed to study nanometer scale mechanical properties of grain boundaries in nanocrystalline FCC metals. The nonlinear field projection is based on the principle of virtual work, for virtual variations of atomic positions in equilibrium through nonlocal interatomic interactions such as EAM potential interaction, to get field-projected subatomic-resolution traction distributions on various grain boundaries. The analyses show that the field projected traction produces periodic concentrated compression sites on the grain boundary, which act as crack trapping or dislocation nucleation sites. The field projection was also used to assess the nanometer scale failure processes of Cu Σ5 grain boundaries doped with Pb. It was revealed that the Pb dopants prevented the emission of dislocations by grain boundary slip and embrittles the grain boundary.

INTRODUCTION

Nanocrystalline materials are polycrystals with nanometer-scale grain sizes, and have been the subject of widespread research over the past few decades. There is now general consensus among the scientific community that the mechanical strength and toughness of these nanocrystalline materials are structurally characterized by their large volume fraction of grain boundaries. However, the intrinsic relationship between the nanometer scale mechanical properties of grain boundaries and their macroscopic failure behavior are still not well understood. Studies have attempted to ascertain the strength characteristics of grain boundaries and the effects of dopants on grain boundary embrittlement via their electronic structure changes and local density of states [1,2]. However, these ab-initio calculations cannot quantitatively characterize the mechanical strength and toughness of the grain boundary, since the fracture energy of the grain boundary is dependent on the separation process [3-5]. Therefore, an accurate assessment of the nanometer scale failure processes of the grain boundaries is required to characterize the mechanical strength of nanocrystalline materials.

Despite the availability of computational tools such as molecular dynamics simulations, determination of the grain boundary traction-separation characteristics is highly nontrivial due to the discreteness of the atomic system which results in inconsistencies in the definition of stress. In molecular dynamics, for example, the virial stress is widely used to interpret physical continuum properties. Figure 1 shows the interpolated σ_{22} virial stresses along a Σ5 symmetric tilt grain boundary in Cu, connected by linear interpolation. Observe that the linear interpolation of conventional virial stress distribution do not satisfy the basic equilibrium requirement in the absence of far-field loading, i.e. sum of forces = 0. Therefore, to assess the strength and the toughness of the grain boundaries, we must have proper field representation of the grain boundary which satisfies balance laws.

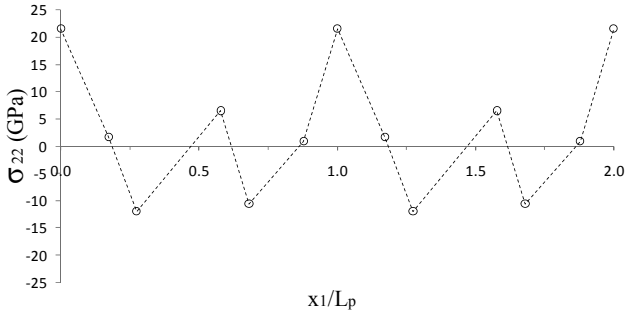

Figure 1. Interpolated virial stresses along a $\Sigma 5$ symmetric tilt grain boundary in pure copper.

THEORY

We present a new method of projecting the nonlinear grain boundary stresses from the nonlocal deformation field. Central to this nonlinear field projection method is the principle of virtual work

$$\int_V \delta\boldsymbol{\varepsilon}:\boldsymbol{\sigma}\,\mathrm{d}\upsilon = \int_S \delta\mathbf{u}\cdot\mathbf{t}\,\mathrm{d}s = \Delta\Phi \tag{1}$$

for a static system without body forces. Here $\delta\boldsymbol{\varepsilon}$ is the virtual strain work-conjugate to the Cauchy stress $\boldsymbol{\sigma}$, $\delta\mathbf{u}$ denotes an admissible virtual displacement field, $\mathbf{t}$ represents the boundary traction, and $\Delta\Phi$ is the variation of the total interatomic potential energy. A schematic of the grain boundary model is shown in Fig. 2. We divide the model into five regions, D_1, D_2, D_3, D_0 and D_u, where D_1, D_2 and D_3 make up the volume V with bounding surface S. The common interface between D_2 and D_u lies along the grain boundary ($x_2 = 0$), where the tractions are to be determined. These tractions are expressed in terms of the Fourier series

$$t(x_1,0) = \sum_{k=1}^{\infty} A_k \sin\frac{2k\pi x_1}{L_p} + \sum_{k=0}^{\infty} B_k \cos\frac{2k\pi x_1}{L_p} \tag{2}$$

where L_p is the periodic length of the grain boundary, k the wave number, and A_k and B_k are the Fourier coefficients to be determined. The virtual displacement field in V is define as

$$\begin{aligned} &\delta\mathbf{u}^1(x_1,x_2) = \varepsilon F(x_1,x_2)\sin\frac{2k\pi x_1}{L_p} \\ \text{or}\quad &\delta\mathbf{u}^2(x_1,x_2) = \varepsilon F(x_1,x_2)\cos\frac{2k\pi x_1}{L_p} \end{aligned} \tag{3}$$

where ε is the amplitude of displacement variation. The perturbation-displacement envelope function $F(x_1,x_2)$ is defined as

$$F(x_1,x_2)=\begin{cases}1, & \text{for } (x_1,x_2)\in D_u\\ 0, & \text{for } (x_1,x_2)\in D_0\\ \left(\frac{H}{x_2}-1\right)\left(1+\frac{2x_1}{L}\right), & \text{for } (x_1,x_2)\in D_1\\ \left(1-\frac{x_2}{H}\right), & \text{for } (x_1,x_2)\in D_2\\ \left(\frac{H}{x_2}-1\right)\left(1-\frac{2x_1}{L}\right), & \text{for } (x_1,x_2)\in D_3.\end{cases} \tag{4}$$

where L is the width and H is the height of the domain V. This continuous function has unit value along the grain boundary interface between D_2 and D_u but decays smoothly to zero at the other boundaries, as shown in Fig. 2. Then, substituting (2), (3) and (4) in (1), we obtain

$$A_k=\frac{2\Delta\Phi_k^1}{\varepsilon\, L} \quad \text{or} \quad B_k=\frac{2\Delta\Phi_k^2}{\varepsilon\, L}. \tag{5}$$

where $\Delta\Phi_k^{1,2}$ represent the total interatomic potential energy variation caused by $\delta\mathbf{u}^{1,2}$ in (3).

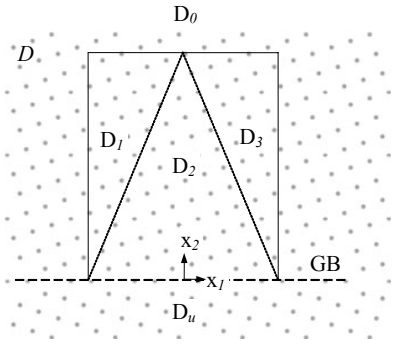

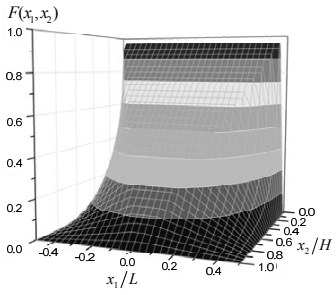

Figure 2. Calculation domain for nonlinear field projection (left). Perturbation-displacement envelope function $F(x_1,x_2)$ (right).

DISCUSSION

The above nonlinear field projection scheme is used to determine the grain boundary tractions in pure Cu, and Cu doped with Pb. The energetics of the molecular interactions was evaluated using the Embedded Atom Method potential in the classical molecular dynamics simulation package LAMMPS [6].

Sub-atomic grain boundary tractions

Figures 3 and 4 show the projected tractions along Σ5 and Σ13 symmetric tilt grain boundaries in pure Cu. Our numerical experiments show that the projected grain boundary traction distribution is independent of the height and width of the domain *D*, and rapidly converges after about twelve Fourier terms (i.e. six sine and cosine terms respectively), which demonstrates the overall stability of the numerical scheme. These projected tractions satisfy force balance, i.e. zero net vertical forces in the absence of far field loading, unlike the linearly interpolated virial stresses. At the discrete atomic sites, the projected stresses are in good agreement with the virial stress values. However, the projected tractions along the grain boundary are highly oscillating, and one cannot readily infer the stress distributions in between atoms by simple interpolation of the virial stress.

Within each grain boundary period, our projected stresses for Cu Σ5 grain boundary show a compressive peak stress of -18 GPa compared to the virial stress prediction of -13 GPa. For the Cu Σ13 grain boundary, the peak compressive stresses are even higher at -65 GPa, compared to the virial stress prediction of -25 GPa. Hence, the virial stress predictions severely underestimate the actual peak compressive stress which occurs in between atoms. The periodic compressive pinching stress is responsible for crack trapping and grain boundary toughening during intergranular fracture [7], and cannot be captured by simple virial stress interpolation.

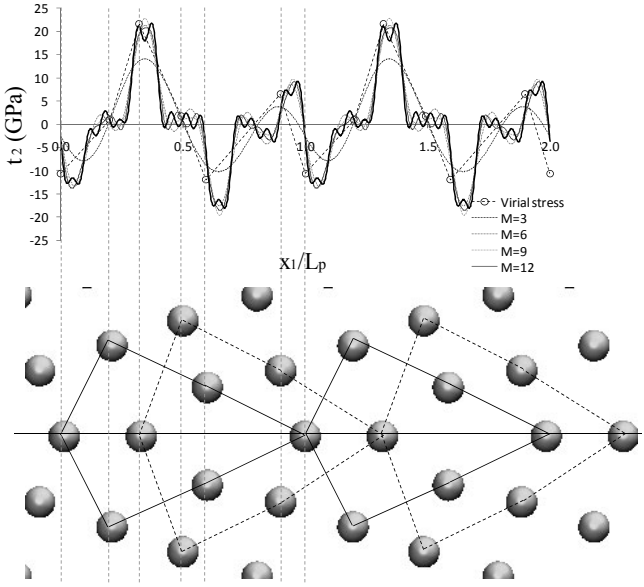

Figure 3. Traction distribution along pure copper Σ5 grain boundary.

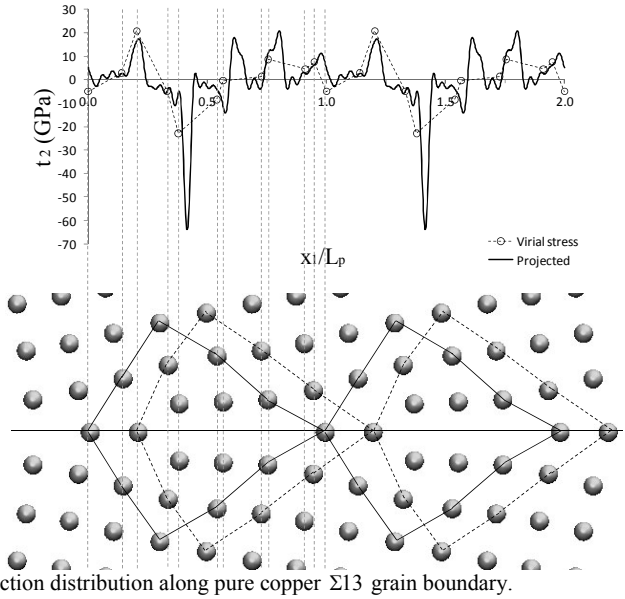

Figure 4. Traction distribution along pure copper $\Sigma 13$ grain boundary.

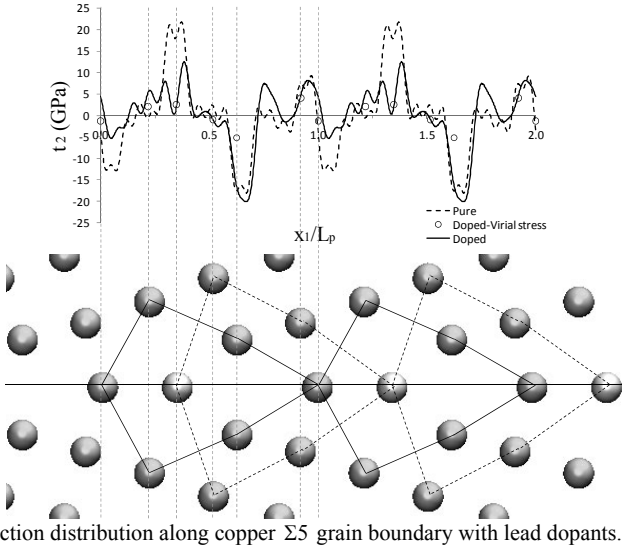

Figure 5. Traction distribution along copper $\Sigma 5$ grain boundary with lead dopants.

Grain boundary embrittlement by doping

Figure 5 shows the effects of Pb doping on the embrittlement of Cu Σ5 grain boundary. The bold line denotes the projected grain boundary tractions for Pb doped Cu, while the traction distribution for pure Cu Σ5 grain boundary is shown by the dashed line. Molecular statics simulations based on the conjugate gradient method reveal that the minimum energy configuration consists of Pb dopant atoms which substitute pre-existing Cu atoms along the grain boundary at the high tensile stress site within each grain boundary period. The presence of these dopant atoms significantly reduces the peak grain boundary traction from 20 GPa to 12 GPa, and also reduces the neighboring compressive peak from -15 GPa to -5 GPa.

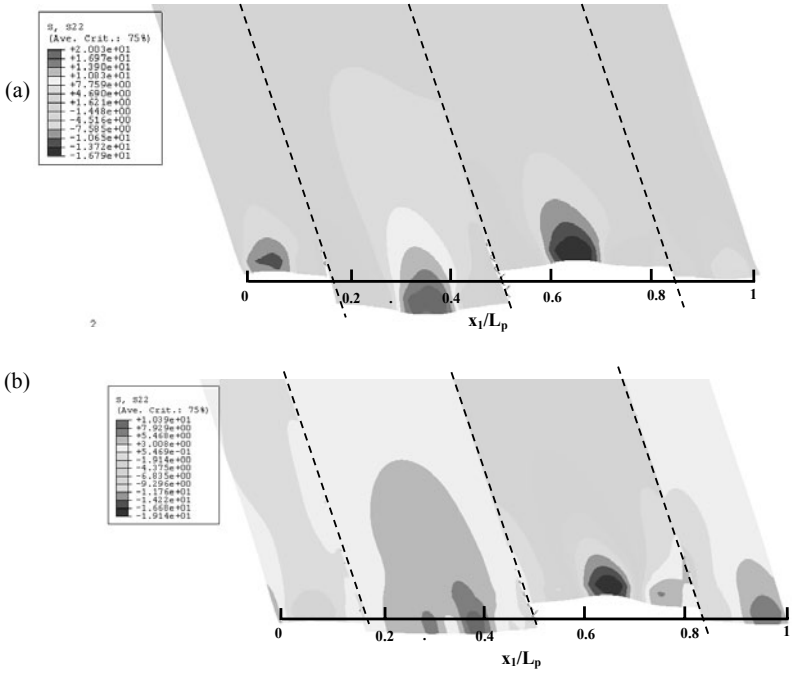

Figure 6. The deformed grain boundary configuration and the σ_{22} stress field for Σ5 grain boundary of (a) pure copper and (b) lead doped copper. The dashed lines denote possible dislocation glide planes.

Figure 6 depicts the elastic stress fields caused by Σ5 grain boundary tractions for pure Cu and Pb doped Cu. The dashed lines denote the possible pathways for grain boundary dislocation emission or absorption, and are modeled using cohesive zone laws calibrated by the

generalized stacking fault energies of Cu. In the absence of external loading, the grain boundary tractions can induce an initial "opening" of the grain boundary, i.e. a non-zero initial separation for zero initial applied traction. The initial separation is much larger for the pure Cu grain boundary than for Pb doped Cu, due to the reduction in the tensile and compressive stress peaks in the presence of Pb dopants as earlier shown in Fig. 5. The smaller initial grain boundary separation for Pb doped Cu infers that the emissivity of dislocations is suppressed.

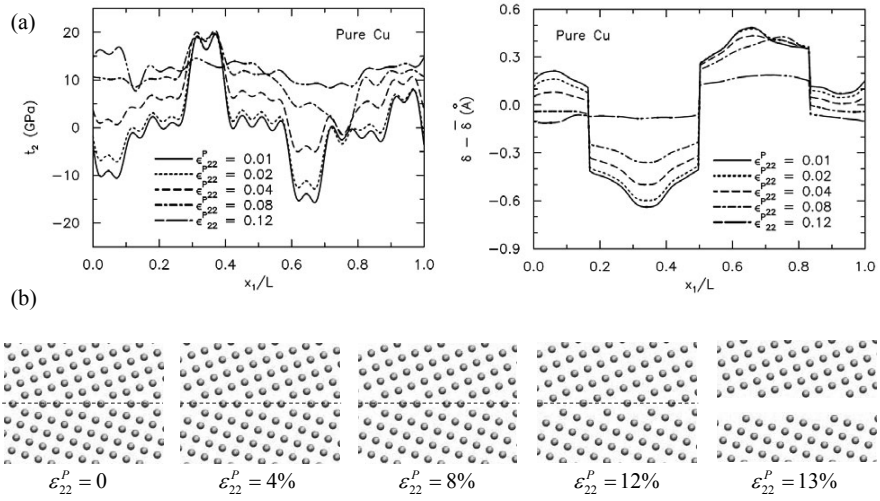

Figure 7. (a) Evolution of cohesive tractions and total separation variations and (b) atomic configurations for $\Sigma 5$ grain boundary of pure copper.

Figure 7a shows the development of cohesive tractions and total separation variations along pure Cu $\Sigma 5$ grain boundary under uniaxial straining ε^P_{22}. The separation variations are obtained by applying the traction variations along the grain boundary to the elastic half-space shown in Fig. 6. The corresponding atomic configurations are shown in Fig. 7b. Observe that under globally applied uniaxial strains of $\varepsilon^P_{22} \le 0.08$, the cohesive traction and separation distribution along the grain boundary evolves in proportion with the applied load, which indicates that the atomic configuration near the grain boundary is unchanged. At higher applied strains of $\varepsilon^P_{22} = 0.12$, the shape of the traction and separation profiles changes radically, suggesting that atomic rearrangement of the grain boundary has taken place. At this stage, local instabilities resulting in periodic grain boundary partial dislocation emissions in the upper grain are observed, with the lower grain remaining unchanged. Final grain boundary separation occurs at $\varepsilon^P_{22} = 0.13$. These changes in the atomic configurations by dislocation emission imply ductility of the material, and prohibit the use of the classical Griffith cleavage energy concept [5].

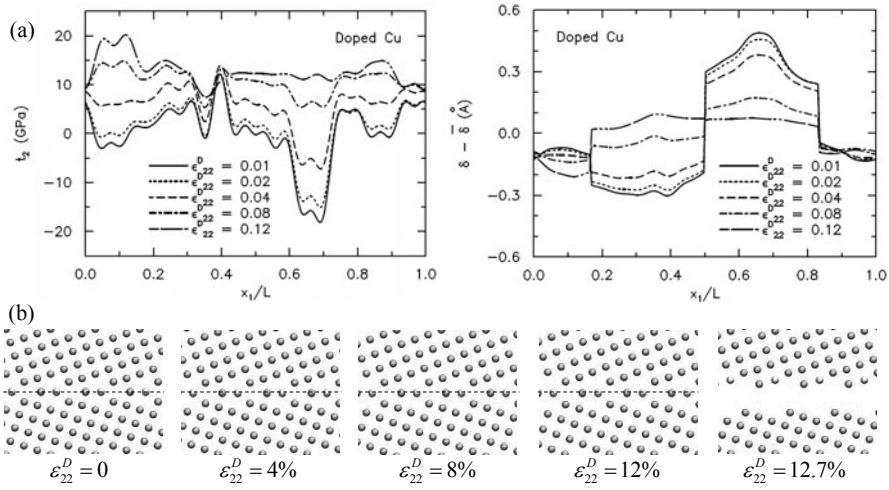

Figure 8. (a) Evolution of cohesive tractions and total separation variations and (b) atomic configurations for Σ5 grain boundary of lead doped copper.

The evolution of cohesive tractions and total separation variations along Pb doped Cu Σ5 grain boundary under uniaxial straining ε^D_{22} is shown in Fig. 8a, with snapshots of the corresponding atomic configuration evolution displayed in Fig. 8b. Unlike the pure Cu grain boundary, no atomic rearrangement or dislocation emission was observed even at $\varepsilon^D_{22} = 0.12$, which is close to the failure strain of $\varepsilon^D_{22} = 0.127$. The absence of plastic deformation suggests that the locking effect of Pb dopants prevent grain boundary sliding.

While the global failure strains of both pure Cu and Pb doped Cu Σ5 grain boundaries are similar, their local failure response or fracture energy can be vastly different. To quantitatively characterize the average traction-separation relationship of the grain boundary, we linearly extract the local average separation of the grain boundary $\bar{\delta}$ from the average bulk stress $\bar{\sigma}$ in the far-field and the global applied strain $\varepsilon^{\mathrm{A}}_{22}$, and obtain $\bar{\delta} = \left(\varepsilon^{\mathrm{A}}_{22} - \bar{\sigma}/E^*\right)h$. Here, E^* is the effective elastic modulus of the crystal and h the height of the simulation domain from which the global strain $\varepsilon^{\mathrm{A}}_{22}$ is calculated. The superscript A in $\varepsilon^{\mathrm{A}}_{22}$ is denoted by P for pure Cu or D for Pb doped Cu. Figure 9 shows the average traction $\bar{\sigma}$ versus local separation $\bar{\delta}$ profiles for pure Cu and Pb doped Cu Σ5 grain boundaries. Observe that while the peak $\bar{\sigma}$ for both pure Cu and Pb doped Cu are similar, their local separations $\bar{\delta}$ are dramatically different beyond $\varepsilon^{\mathrm{A}}_{22} = 0.08$, with the pure Cu grain boundary exhibiting a much longer separation for the same global applied strain. This critical strain level denotes the point at which atomic rearrangement of the pure Cu grain boundary occurs, resulting in the emission of partial dislocations at periodic grain boundary

sites. In contrast, no such grain boundary rearrangement or dislocation emission is observed for Pb doped Cu grain boundary. Consequently, a nearly two-fold reduction in the grain boundary toughness is observed in the presence of Pb dopants, which leads to embrittlement of the material.

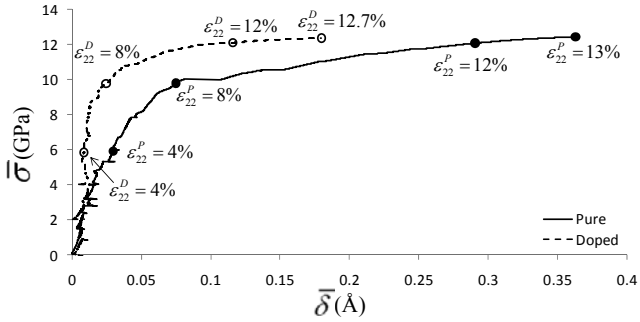

Figure 9. Traction-separation relationship for pure and Pb doped Cu $\Sigma 5$ grain boundary.

CONCLUSIONS

A field projection of grain boundary that satisfies balance laws has been developed. The field projection was used to assess the grain boundary cohesive zone characteristics for its separation process. It is found that the atomic rearrangement during the separation process causes local instabilities which prohibit the use of the classical cleavage energy concept. Dislocation emission results in significant atomic rearrangement and can be gauged by configuration forces. Since dislocation emission requires local grain boundary slip, the locking of local grain boundary slip by Pb dopants embrittles the grain boundary.

ACKNOWLEDGMENTS

The supports of U.S. NSF through MRSEC/Brown (DMR0079964) and KIST through Hybrid Computational Science Laboratory / Brown are gratefully acknowledged.

REFERENCES

1. Duscher, G., Chisholm, M.F., Alber, U. & Ruhle, M. *Nature Materials* **3**, 621-626 (2004).
2. Schweinfest, R., Paxton, A.T. & Finnis, M.W. *Nature* **432**, 1008-1011 (2004).
3. Rice, J.R. *J Mech Phys Solids* **40**, 239-271 (1992).
4. Li, Q. & Kim, K.-S. *Acta Mechanica Solida Sinica* **22**, 377-390 (2009).
5. Griffith, A.A. *Philos Trans Roy Soc Lond A* **221**, 163-198 (1921).
6. Plimpton, S.J. *J. Comp. Phys.* **117**, 1-19 (1995).
7. Cheng, Y., Jin, Z.-H., Zhang, Y.W. & Gao, H. *Acta Mater* **58**, 2293-2299 (2010).